

Numerical Analysis of Carbon Deposition in an Internal Methane Reforming SOFC with Anode Gas Recycling

Valérie Eveloy

Department of Mechanical Engineering, The Petroleum Institute, Abu Dhabi, U.A.E.
veveloy@pi.ac.ae

Abstract

The development of solid oxide fuel cell (SOFCs) systems capable of direct internal reforming (DIR) of methane is being actively pursued. However, a major challenge with current state-of-the-art nickel-based anodes is their propensity to form deteriorous carbon deposits in DIR, unless excess steam is introduced in the fuel. Reduced fuel humidification levels are desirable from the viewpoints of cell performance, reliability and plant economics. This study explores the use of partial recycling of the anode exhaust as a mitigation strategy against carbon deposits at fuel steam-to-carbon ratios less than unity. Using a detailed computational fluid dynamics (CFD) model which couples momentum, heat, mass and charge transport with electrochemical and chemical reactions, the spatial extent of carbon deposition within a SOFC anode is analyzed by accounting for both the cracking and Boudouard reactions, for several fuel humidification and recycling conditions. At temperatures of approximately 1173 K and for inlet fuel molar H₂O/CH₄ ratios between 0.5 and 1, 50% (mass %) fuel recycling is found to be an effective strategy against carbon deposition. For lower recycling levels at the same fuel compositions, or lower fuel humidification levels (regardless of the recycling level), fuel recycling reduces the risk of coking, but does not eliminate it. The analyses presented suggest that recycling of the anodic fuel stream could help extend the operational range of DIR-SOFCs to lower fuel humidification levels than typically considered, with reduced risks of carbon deposits, while reducing system cost and complexity in terms of steam production. For dry or weakly humidified fuels, additional mitigation strategies would be required.

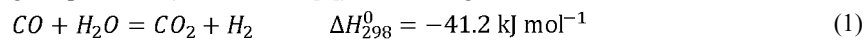
1. Introduction

The requirement for energy sustainability and environmental issues are prompting the development of new energy generation and utilization systems. In recently published roadmaps for the transition to a hydrogen-oriented economy, fuel cells are considered a key enabling technology [1]. Considering their fuel flexibility, efficiency, suitability to high-temperature waste heat utilization, and low pollutant emissions, solid oxide fuel cells (SOFCs) are an attractive technology for power generation [2-4]. Methane has generally been considered the fuel of choice for SOFCs, given the abundance of natural gas and its production and distribution infrastructure, in contrast with hydrogen [2,3,5,6]. Rather than converting methane to electrochemically active hydrogen in a reformer or partial oxidation (POx) reactor, either prior to entering the fuel cell stack [3,7], or in a separate stack compartment via indirect internal reforming (IIR) [8], the development of SOFC anodes that support direct internal reforming (DIR) [9-13], is being actively pursued. DIR could enable plant simplifications by reducing the constraints on a separate fuel pre-processor, or possibly fully eliminate the need for it. In addition, DIR could also lower the requirement for stack cooling, since methane reforming is a strongly endothermic reaction.

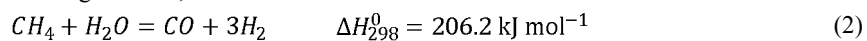
However, a major barrier to SOFC operation on methane and higher hydrocarbons is carbon deposition [2,14]. This paper summarizes current challenges associated with carbon deposition in DIR-SOFCs, and explores the effectiveness of partially recycling the anode exhaust stream as a coking mitigation strategy. This is achieved using a detailed computational fluid dynamics (CFD) model of cell behavior and thermodynamic analysis of carbon deposition.

2. Carbon Deposition in DIR-SOFCs

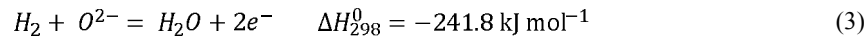
At SOFC operating temperatures (923 – 1273K [2]), the water-gas-shift reaction,



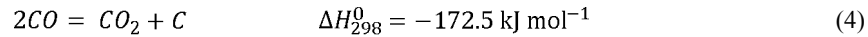
and methane steam reforming reaction,



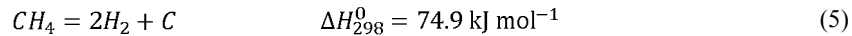
can be supported by catalysts such as nickel in commonly-used nickel-yttria-stabilized zirconia (Ni-YSZ) anodes¹ [10,15], to generate the hydrogen necessary for the electrochemical reaction,



The heat produced by the electrochemical reaction (3) can be utilized by the endothermic steam reforming reaction (2). Reaction (3) also contributes to drive reaction (2) by consuming hydrogen as it is formed [4]. The Boudouard reaction,



which is also catalyzed by nickel [10], and methane cracking reaction,



are major pathways of carbon formation at high SOFC operating temperatures [16,17]. DIR typically requires the addition of steam to the fuel in excess of the stoichiometric coefficient² of reaction (2). This displaces the equilibrium of reaction (1) towards the production of CO₂ rather than CO, thereby hampering carbon deposition via the Boudouard reaction (4). Carbon deposits are most prevalent in the vicinity of the anode inlet, where little hydrogen is present, and where the rate of carbon formation exceeds its rate of removal. Carbon deposition is a critical problem for SOFCs operating on hydrocarbons, as it can impede gas flow and block active sites on the anode. In extreme situations, it can result in the growth of carbon filaments that can generate considerable mechanical stresses within the electrode structure [4].

However, the addition of large quantities of steam to the fuel to sustain internal reforming and impede carbon deposition is associated with several difficulties. High levels of fuel humidification increase system cost and complexity in terms of steam production, reduce the open circuit voltage, can deteriorate the nickel catalytic activity due to sintering of the nickel particles, and favorize significant temperature gradients within the membrane-electrode-assembly (MEA) [4]. Temperature gradients arise from the rapid kinetics of the strongly endothermic steam reforming reaction and the exothermic electrochemical reaction, which are spatially separated within the anode structure. The stresses induced by differential thermal expansion can be detrimental to stack reliability [18]. These considerations are driving hydrocarbon fuel requirements towards lower steam content [6], with greater risks of carbon deposition.

In this regard, Vernoux *et al.* [19] proposed the concept of gradual internal reforming (GIR), which is similar to DIR, but involves the addition of significantly lower quantities of steam (steam-to-carbon (S:C) ratios < 1). In this approach, the steam required for reforming is essentially generated in-situ by the electro-chemical reaction. George *et al.* [20] and Klein *et al.* [21] explored the feasibility of GIR operation experimentally and numerically, respectively, for Ni-YSZ based SOFCs operating on humidified methane mixtures. Reducing the S:C ratio below 1 was shown to enable a delocalization of the reforming reaction in the cell length direction, which resulted in improved thermal coupling of the reforming and electrochemical reactions [21]. However, increased risks of carbon deposits were highlighted relative to DIR [17,21].

Attempts to resolve the problem of carbon deposition have investigated novel anode architectures [22] and the impact of operating conditions. In terms of anode design, solutions proposed include the use of metal dopants (e.g., gold, copper, ruthenium, molybdenum), cermet inhibitors to carbon deposition (e.g., ceria) [4,23,24], and anode barrier layers [25]. However, the costs associated with alternative materials can be prohibitive [23]. With regard to anode barrier layers, carbon formation may still occur during start-up transients where steam is insufficiently generated electrochemically, and careful design of low-resistance current collecting paths may be required for tubular cells [25]. In terms of operating conditions, high current density [26], high hydrogen-to-carbon ratio [23], and lower temperature [22] have been shown to reduce carbon deposits. However, adjusting these parameters to reduce carbon deposition may not be compatible with other operating requirements. In summary, no fully satisfactory solution has yet been identified to reliably sustain internal methane reforming at low fuel humidification levels.

Another approach is considered here, which has been marginally considered in previous cell-level studies that have analyzed carbon deposition, and consists in partially recycling the anode exhaust gas. This strategy has the potential to mitigate carbon deposition as well as temperature gradients, while lowering system requirements in terms of steam production.

3. Anode Gas Recycling

Fuel recycling consists in separating a fraction of the SOFC anode exhaust and mixing it with the inlet fuel, either upstream of a pre-reforming unit [3,5,27] or upstream of the cell fuel channel [18,28-30]. Since

¹ Currently, the preferred SOFC electrolyte material is dense yttria (Y₂O₃)-stabilized zirconia (ZrO₂) (YSZ). In conjunction with YSZ, a porous nickel-zirconia (Ni-ZrO₂) cermet is the most common anode material, while the cathode is typically a lanthanum manganite (LaMnO₃) based material [4,6].

² Steam-to-carbon (S:C) ratios of 1 to 3 are typically employed to avoid coking on conventional nickel-based anodes [4].

this paper focuses on DIR and system design is not its aim, the recycled fuel is mixed with the anode inlet stream, rather than upstream of a pre-reformer.

Qualitatively, the impact of fuel recycling on cell operation may be anticipated as follows. In the absence of anode stream recycling, the exhaust gas of methane fueled SOFCs (e.g., wet or dry methane, or methane containing syngas) may typically contain steam (H_2O), CO_2 , CO , and both unconverted H_2 and CH_4 [31]. Partial recycling of the anode exhaust therefore enriches the inlet fuel in H_2O , CO_2 , H_2 and CO while reducing its CH_4 fraction. H_2 enrichment increases the current density at inlet, which in turn favors carbon removal through in-situ steam production. Higher H_2 content also impedes the carbon cracking reaction (5), while CO_2 enrichment favors carbon removal through the reverse Boudouard reaction (4). Increased electrochemical activity and reduced reforming activity at the fuel cell inlet contribute to lower temperature gradients in the cell length direction. Furthermore, steam recycling would reduce or possibly eliminate the need for separate steam production.

Recent plant-level numerical studies (for example, [27]) have analyzed the effect of fuel recycling on system efficiency. However, few experimental [5] or numerical investigations [18,28-30] have explored fuel recycling at cell level. In general, these studies have shown promising results in terms of reduced MEA temperature gradients [5,18,29,30]. Peters *et al.* [5] experimentally observed that CO_2 enrichment of the fuel due to anode gas recycling led to decreased catalytic activity, while for temperatures higher than 1000 K, H_2 enrichment increased the CH_4 conversion rate. The primary purpose of recycling was to recover waste heat from the anode exhaust to sustain external pre-reforming and eliminate the need for separate steam production. The amount of recycling was balanced in such a manner that steam for reforming was totally recovered from the SOFC. Colpan *et al.* [28] found that the negative effects of fuel recycling, in terms of reduced cell voltage [18,28,29] due to fuel enrichment in inert gases, and reduced cell power output [28] and efficiency [18,28], are not significant at low current density, compared to the effects of the fuel utilization ratio. Furthermore, these negative effects can be compensated by system efficiency improvements, as a result of reduced constraints on external steam production [18]. Finally, fuel recycling reduces the fuel utilization ratio due to increased mass flow [28], which should result in more uniform current density [18].

However, the above cell-level analyses of fuel recycling [5,18,28-30] have focused on highly humidified methane (S:C ratios ≥ 2). Consequently, little consideration has been given to the potential benefits of fuel recycling in terms of mitigating the risks of carbon deposition. For humidified methane having an inlet S:C of 2, Nikooyeh *et al.* [30] analyzed the variation in inlet fuel composition and average current density as a function of the fuel recycling ratio. The H_2O/CH_4 ratio at the cell inlet was found to remain unchanged for 50% and 60% recycling, while the average current density increased. At 75% recycling, the inlet H_2O/CH_4 ratio increased to approximately 4, which would be advantageous in terms of carbon removal, but current density decreased. It was concluded that an optimum level of fuel recycling may exist depending upon system parameters. However, the possibility of carbon deposition was considered only on the basis of the fuel inlet H_2O/CH_4 ratio, with no other thermodynamic considerations.

In summary, no numerical cell-level study has quantified the effects of fuel recycling on carbon deposition other than by analyzing the inlet H_2O/CH_4 ratio [30], nor has considered weakly humidified methane fuels (S:C < 1). Furthermore, such studies [18,28-30] have employed various levels of modeling approximations, such as zero-dimensional modeling [28], representation of electrode activation overpotentials using effective charge transfer resistances [18], equilibrium assumption of the water-gas-shift reaction [18], omission of gas-phase chemistry [30], restriction of the triple phase boundary to the electrode/electrolyte interface [18,30], and channel wall convective heat transfer modeled using semi-empirical heat transfer coefficients [29,30].

In the present study, a detailed CFD model is used to undertake a thermodynamic analysis of carbon deposition in a SOFC operated at low fuel S:C ratios (0.1 to 1), where significant risks of coking exist. The objective is to provide an estimate of the spatial extent of carbon deposits, which would be difficult to obtain in-situ experimentally without post-electrochemistry destructive testing.

4. Test Configuration and Methodology

The test configuration employed to evaluate the potential effectiveness of fuel recycling in mitigating carbon deposits in internal reforming SOFCs is based on that previously employed by Klein *et al.* [21] to investigate the feasibility of GIR, but fuel recycling was not considered. The MEA consists of an electrolyte-supported planar structure, represented in Figure 1. The electrolyte, anode and cathode materials are YSZ, porous Ni-YSZ and porous lanthanum manganite ($La_{0.7}Sr_{0.3}MnO_3$), respectively. The thicknesses of these parts are listed in Table 1. As in [21], the analyses presented focus on the first 30 mm of cell length, which would be most prone to coking. The anode and cathode channels are fed in a co-flow configuration with humidified methane and air, respectively.

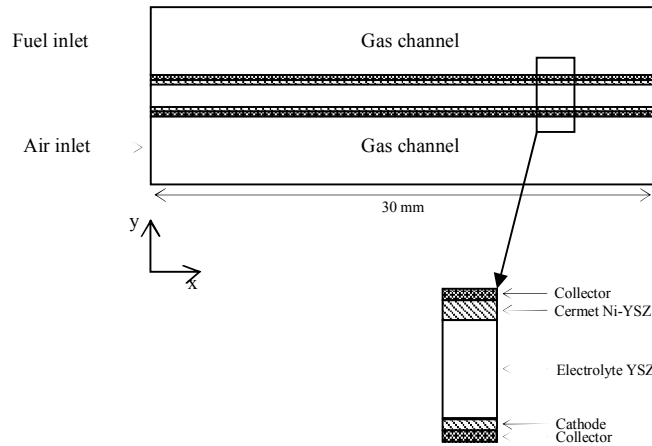


Figure 1. GIR-SOFC configuration, based on [21].

Table 1. Geometric parameters of the SOFC, Figure 1 [21].

Geometry	Thickness (mm)
Gas channel (x2)	3.00
Anode	0.20
Electrolyte	1.00
Cathode	0.10
Collector (x2)	0.10

Given the requirement for hydrocarbons fuels with lower steam content [6], base inlet fuel compositions (i.e., prior to recycling) with molar H_2O/CH_4 ratios ranging from 0.1 to 1 are considered (a ratio of 1 delineates the boundary between GIR and DIR [21]). In order to apply the same molar flow rate of methane for all inlet fuel compositions, the flow rate of the fuel mixture is varied (Table 4).

Before exploring the effect of fuel recycling, the model predictions are compared with those presented by Klein *et al.* [21] using a different CFD software for inlet fuel compositions corresponding to $H_2O/CH_4=1$ and 0.1, at an inlet fuel temperature 1173 K and current density of $0.34 A/cm^2$.

The propensity to carbon deposition is then assessed at the same inlet fuel temperature, for inlet H_2O/CH_4 ratios of 0.1, 0.5 and 1.0, and fuel recycling ratios from 20% to 80% (mass %). This is achieved based on the thermodynamic analysis presented by Hou and Hugues [32] and applied by Klein *et al.* [17,21] to DIR- and GIR-SOFCs. The possible direction of a reaction can be evaluated from its reactional quotient and equilibrium constant. The driving forces for carbon deposition, accounting for the Boudouard and methane cracking reactions, are defined as:

$$\alpha = \frac{Q_B}{K_B} = \frac{P_{CO_2} a_c}{P_{CO}^2 K_B} \quad (6)$$

where Q_B and K_B are the reactional quotient and equilibrium constant of the Boudouard reaction (K_B decreases as temperature rises), a_c is the carbon activity and is taken as 1 for the calculations, and

$$\beta = \frac{Q_C}{K_C} = \frac{P_{H_2}^2 a_c}{P_{CH_4} K_C} \quad (7)$$

where Q_C and K_C are the reactional quotient and equilibrium constant of the methane cracking reaction, respectively. If $\alpha < 1$ or $\beta < 1$, the Boudouard or methane cracking reaction, respectively, will proceed to the right, and carbon deposition is thermodynamically possible. The spatial distributions of α and β within the anode structure are numerically predicted based on the local species partial pressures, and the local values of the temperature-dependant equilibrium constants K_B and K_C , using the CFD model described in the following section.

In situations where $\alpha < 1$ and $\beta > 1$ (or vice versa), the combined effect of the two reactions needs to be considered. This effect may be evaluated based on the following coefficient [17]:

$$\gamma = \alpha \beta \quad (8)$$

Thus, a value of γ less than 1 indicates the possible presence of carbon within the anode. It is acknowledged that this criterion does not provide information on the amount and rate of carbon deposition. However, as these quantities are difficult to predict quantitatively [33], thermodynamic predictions can provide useful qualitative guidance [31]. In this instance, the methodology employed permits regions of

the anode where carbon deposits are thermodynamically favored, to be identified and compared for several fuel compositions, both in recycling and non-recycling conditions.

5. Computational Model

The numerical model was constructed and solved using COMSOL Multiphysics Version 3.4 [34], a commercially-available CFD software for the modeling of multiphysics phenomena utilizing finite-element methods (FEM).

The modeling methodology is based on that previously implemented by Klein *et al.* [21] in a different, finite-volume CFD code. Mass, heat and charge transport, coupled with electrochemical and chemical reactions are incorporated. The cell is fed with CH₄/H₂O mixtures of different compositions and air at the anode and cathode channels, respectively. The following assumptions are made:

- i. Two dimensional geometry, as defined by the cell length and thickness directions
- ii. Steady state, non-isothermal conditions
- iii. Solid state materials have homogenous and isotropic physical properties
- iv. The gas mixtures are considered as ideal gases
- v. Channel flow is laminar
- vi. Mass transport in the porous electrodes is modeled using a combination of Maxwell Stefan diffusion, Knudsen diffusion and convective transport. The electrolyte layer is modeled as fully impermeable to mass transport, given its small porosity, $\varepsilon = 0.01$.
- vii. Fuel consumption results from both internal reforming in the porous anode and the water-gas-shift reaction in both the porous anode and fuel channel. Both reactions are modeled using previously reported kinetic expressions [32,35].
- viii. The conversion of CO to H₂ by the shift reaction provides an important source of H₂. Since indirect utilization of CO generally exceeds its utilization by direct electrochemical conversion [36], H₂ is considered the only electrochemically active species.
- ix. Unlike in the majority of SOFC CFD models previously published, where electrochemical reactions are confined to the electrode/electrolyte interfaces, the triple phase boundaries (TPB) are considered uniformly distributed in each electrode volume. This approach is realistic, considering electrode thickness (10 μm and 20 μm for the cathode and anode, respectively) [37].
- x. The ohmic drop within the cell is due to the ionic resistance of the electrolyte, and both the ionic and electronic resistances of the electrodes. The ionic and electronic conducting phases are homogeneous. No ohmic resistance is assumed within the interconnects, which have a uniform potential and are modeled as planar surfaces.
- xi. The cell is assumed to operate under adiabatic conditions, which is representative of the thermal environment of a unit cell in a central region of a stack [29].

Governing equations

In the gas flow channels, a weakly compressible form of the steady-state Navier Stokes equations (9 and 10) [34] is employed, which accounts for variations in fluid density associated with fluid composition, pressure and temperature. Mass conservation is thus described as:

$$\nabla \cdot (\rho \mathbf{v}) = 0 \quad (9)$$

The momentum conservation equation, with turbulence, volume forces, and dilatational viscosity omitted, is expressed as:

$$\rho(\mathbf{v} \cdot \nabla)\mathbf{v} = \nabla \cdot [-p\mathbf{I} + \mu(\nabla\mathbf{v} + (\nabla\mathbf{v})^T) - \frac{2\mu}{3}(\nabla \cdot \mathbf{v})\mathbf{I}] \quad (10)$$

Heat transport by conduction and convection may be written as, in absence of viscous heating [34]:

$$\nabla \cdot \mathbf{q} = -j_t \left(\frac{S}{V} \right)_{eff} \eta + \frac{|i \cdot i|}{\sigma} - \rho C_p \mathbf{v} \cdot \nabla T \quad (11)$$

where the heat flux, \mathbf{q} , is due to both thermal conduction and species diffusion:

$$\mathbf{q} = -\lambda \nabla T + \sum_i J_i h_i \quad (12)$$

The first two terms on the right hand side of Equation (11) represent electrical work and Joule heating. The irreversible losses associated with the reactions (conversion of chemical energy to heat) are accounted for through the second term on the right-hand side of Equation (12), as the species i enthalpy, h_i , includes both the enthalpy of formation and the sensible enthalpy. The effective thermal conductivity of the porous medium, λ , accounting for the conductivities of the fluid and solid regions, is calculated as:

$$\lambda = -2\lambda_B + \frac{1}{\left(\frac{\varepsilon}{2\lambda_B} + \lambda_F \right) + \left(\frac{1-\varepsilon}{3\lambda_B} \right)} \quad (13)$$

The species diffusion flux is modeled using multi-component Fickian diffusivities [38]. The combined diffusive and convective transport equation for species i is thus given by [34]:

$$\nabla \cdot \left[-\rho \omega_i \sum_{j=1}^N D_{ik} \left\{ \frac{M}{M_j} \left(\nabla \omega_j + \omega_j \frac{\nabla M}{M} \right) + (x_j - \omega_j) \frac{\nabla P}{P} \right\} + \omega_i \rho \mathbf{v} \right] = R_i \quad (14)$$

In Equation (14), D_{ik} is the ik component of the multi-component Fickian diffusivity matrix, which is calculated from the Stefan Maxwell diffusivity matrix [34,38]. The Stefan Maxwell diffusivities are commonly taken as the binary diffusivities D_{ik} , which in this study are calculated using Chapman-Enskog theory as described in [34,38]. Free molecular and Knudsen diffusion are combined using effective Bosanquet binary diffusion coefficients [39]. Finally, the effective binary diffusivities $D_{ik,eff}$ in the porous electrodes are estimated from the corresponding free-stream diffusivities using the Bruggemann model [40]:

$$D_{ik,eff} = \varepsilon^x D_{ik} \quad (15)$$

In the porous electrodes, the fluid velocity, \mathbf{v} , is derived from Darcy's law,

$$\mathbf{v} = -\frac{\kappa}{\mu} \nabla p \quad (16)$$

and coupled with mass conservation through the continuity equation (17),

$$\nabla \cdot \left(\rho \left(-\frac{\kappa}{\mu} \nabla p \right) \right) = \sum_i \frac{v_i j_{t,i} (S/V)_{eff} M_i}{n_i F} \quad (17)$$

and the species transport equation (14). The mass source term on the right hand side of Equation (17) arises from electrochemical reactions. The methane steam reforming reaction occurs at the surface of a nickel catalyst in the anode. Its reaction rate (kmol m^{-2}) may be modeled using the following Arrhenius expression [32,35]:

$$r_{E1} = 63.6 * T^2 * \exp\left(-\frac{27063}{T}\right) [CH_4][H_2O] - 3.7 * 10^{-14} * T^4 * \exp\left(-\frac{232.78}{T}\right) [CO][H_2]^3 \quad (18)$$

The water-gas-shift reaction occurs both in the gas channel and anode pores. Its reaction rate ($\text{kmol m}^{-3} \text{s}^{-1}$) may be expressed as [32,35]:

$$r_{E2} = 1199 * T^2 * \exp\left(-\frac{12509}{T}\right) [CO][H_2O] - 6.77 * 10^4 * T^2 * \exp\left(-\frac{16909}{T}\right) [CO_2][H_2] \quad (19)$$

The kinetics of the electrochemical reaction within the porous anode,



are described using the Butler-Volmer equation at the triple phase boundary. The anodic current density is expressed as:

$$j_{at} = j_{a0} \left(\exp\left(\frac{\alpha_a F}{RT} \eta_a\right) \frac{[H_2]}{[H_2]_0} - \exp\left(-\frac{\alpha_c F}{RT} \eta_a\right) \right) \quad (21)$$

The anodic overpotential η_a is defined as the difference between the anode electronic (ϕ_{aM}) and ionic (ϕ_{aS}) potentials:

$$\eta_a = \phi_{aM} - \phi_{aS} - E_{a0} \quad (22)$$

and its local values within the electrode are calculated by separately solving the equations for the electronic and ionic charge balances, as outlined below. The reference state at which the equilibrium potential difference between the electronic and ionic conductors is evaluated, E_{a0} , is chosen as the open circuit state (i.e., when no current is produced). At the cathode, oxygen is reduced as:



with a cathodic exchange current j_{ct} obtained from a Butler-Volmer equation similar to Equation (21):

$$j_{ct} = j_{c0} \left(\exp\left(\frac{\alpha_a F}{RT} \eta_c\right) - \exp\left(-\frac{\alpha_c F}{RT} \eta_c\right) \frac{[O_2]}{[O_2]_0} \right) \quad (24)$$

Ionic and electronic currents flow within the ionic (electrolyte) and electronic (nickel catalyst) phases of the porous matrix, respectively. The potential difference between the ionic and electronic phases drives the transfer current. Electrons are transferred from the electrolyte to the catalyst in the anodic layer, and vice versa in the cathodic layer. For an electrochemical reaction occurring at the anode, the governing equations for the ionic and electronic charge balances, according to Ohm's law, may be combined as follows:

$$\nabla \cdot (\sigma_{aS} \nabla \phi_{aS}) = -\nabla \cdot (\sigma_{aM} \nabla \phi_{aM}) = j_{at} (S/V)_{eff} \quad (25)$$

The electrolyte material (YSZ) is a suitable ionic conductor at high temperature but is impermeable to electron flow. Zero electronic current is therefore prescribed in the electrolyte. The potential of this layer follows Ohm's law without any charge creation or consumption:

$$\sigma_{es} \left(\frac{\partial^2 \phi_{es}}{\partial x^2} + \frac{\partial^2 \phi_{es}}{\partial y^2} \right) = 0 \quad (26)$$

For the recycling cases, a fraction of the anode exhaust mass flow is mixed with the incoming fuel. The resulting mass fraction of species i at the fuel channel inlet when a mass fraction R_r of the exhaust fuel is recycled is calculated as [41]:

$$\omega_{i,in,R_r} = \frac{\omega_{i,in,0} + R_r \omega_{i,out,R_r}}{1 + R_r} \quad (27)$$

where ω_{i,in,R_r} and ω_{i,out,R_r} are determined through successive iterations until the convergence criterion described in the following section is met.

Simulation parameters

All material, fluid and kinetic properties are based on those documented in Klein *et al.* [21], with the exception that the porosity and permeability of the dense electrolyte are neglected. The materials properties of the cell constituent elements at 1173 K are listed in Table 2. The dynamic viscosities of the gas species and their mixture are calculated using the kinetic theory of gases [38]. The mass density of the gas mixture follows the ideal gas law. The kinetic data used in the Butler-Volmer equations (reference exchange current density j_0 and symmetry factors α_a and α_c), are listed in Table 3 for both the anode and cathode.

Table 2. Material properties at 1173 K, based on [21].

Element	σ_s [$\Omega^{-1}m^{-1}$]	ϵ [-]	τ [-]	κ [m^2]	λ_B [$Wm^{-1}K^{-1}$]	A/V [m^{-1}]	d_{pore} [m]	σ_M [$\Omega^{-1}m^{-1}$]
Anode Ni-YSZ	5.0	0.4	1.5	$1*10^{-12}$	6.2	$2.2*10^6$	$1*10^{-6}$	$2.9*10^4$
Cathode LaMnO ₃ -YSZ	5.0	0.4	1.5	$1*10^{-12}$	11.0	-	$1*10^{-6}$	$1.0*10^4*$
Electrolyte YSZ	7.0	0	-	0	2.7	-	-	-

Table 3. Kinetic properties for electrochemical reactions [21].

Parameter	Anode	Cathode
(S/V)* j_0 (A m ⁻³)	10^{11}	10^{10}
α_a	0.7	-
α_c	-	0.7

Table 4. Fuel mass flow rates.

xH_2O/xCH_4 (molar)	Anodic flows [kg s ⁻¹]
1.0	$1*10^{-5}$ [21]
0.5	$7.4*10^{-6}$ [Present study]
0.1	$5.2*10^{-6}$ [21]

The potentials of the anodic and cathodic current collectors are prescribed to fixed values, corresponding to a mean current density of 0.34 A cm^{-2} .

The cell is fed with base inlet fuel compositions consisting of humidified methane having H₂O/CH₄ molar ratios of 0.1, 0.5 and 1, at an inlet fuel temperature of 1173 K. In order to apply the same molar flow rate of methane for all fuel compositions, the flow rate of the fuel mixture is varied as described in Table 4. An air mass flow rate of $10^{-3} \text{ kg s}^{-1}$ is applied through the cathode channel to avoid partial depletion of oxygen associated with its reduction. For the recycling cases, fuel mass recirculation ratios ranging from 20% to 80% are imposed.

All computations were performed using Lagrangian quadratic elements on a structured orthogonal mesh containing approximately 8,000 elements. Solution mesh independence was assessed using successive mesh refinement. Fine grid spacings were employed at the cell inlet and outlet, channel/electrode and electrode/electrolyte interfaces to resolve the high gradients of species mole fractions and temperature in these regions, as well as accurately compute the inlet and exhaust fuel compositions for the recycling cases.

Computations were performed using a 3.0 GHz Pentium D processor and 4 GB RAM, operating on Windows XP Professional 64-Bit Edition.

The solutions were considered converged after the relative error, err , defined as the Euclidean norm [34]:

$$err = \left(\frac{1}{N_{dof}} \sum_k^{N_{dof}} |E_k|^2 \right)^{1/2} \quad (28)$$

was reduced to the relative tolerance, which was set to the software's default setting of 10^{-6} . In Equation (28), N_{dof} refers to the number of degrees of freedom, and E_k is the estimated error in the current approximation to the k th component of the true solution vector. The results were found to be minimally altered for values of the relative tolerance lower than 10^{-6} .

6. Results

Before investigating the effect of fuel recycling on the risk of carbon deposition within the anode, the predicted polarization curves in absence of anode gas recycling, for inlet molar fuel compositions of $H_2O/CH_4=1$ and 0.1, are compared with those presented by Klein *et al.* [21] using a different CFD software. As shown in Figure 2, for both fuel compositions the polarization curves predicted with the present model are in good agreement with the corresponding data of [21]. These predictions indicate that cell electrochemical performance is slightly higher in GIR ($xH_2O/xCH_4 = 0.1$) than in DIR ($xH_2O/xCH_4 = 1$), which is attributable to the positive impact of lower steam partial pressure in the fuel on the open-circuit voltage. The good agreement between the present results and those of Klein *et al.* [21] in Figure 2 provides confidence in the numerical model for investigating the effects of fuel recycling.

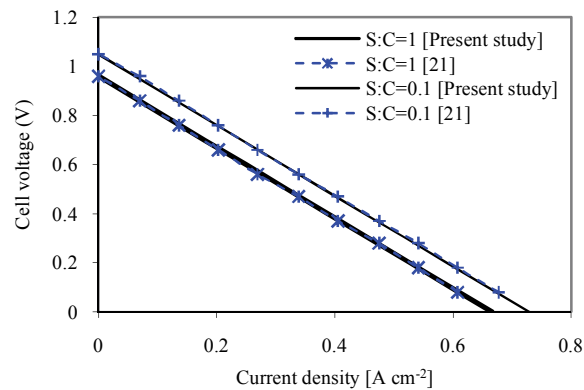


Figure 2. Numerically predicted polarization curves in absence of fuel recycling, for two humidified methane fuel compositions.

The effect of fuel recycling on the susceptibility of the cell to carbon deposition is assessed based on the distribution of coefficient γ in the cell length direction, for inlet xH_2O/xCH_4 ratios of 1, 0.5 and 0.1, in Figures 3, 4 and 5, respectively. Values of γ less than unity delineate regions of the anode where carbon deposition is thermodynamically favored, through the combined effects of the cracking and Boudouard reactions.

Figure 3 suggests that for a xH_2O/xCH_4 ratio of 1 in absence of fuel recycling ($R_r = 0$), carbon deposits only affect a small portion of the cell, restricted to approximately 2.4 mm from the cell inlet. The results of Klein *et al.* [17] for another DIR-SOFC fed with humidified methane at the same xH_2O/xCH_4 ratio are in line with this finding. Accordingly, the profile of coefficient γ , taken along the cell length direction in Figure 3, focuses on the first 5 mm region of the cell. The use of fuel recycling solely to mitigate carbon deposits may therefore not be justified in DIR ($xH_2O/xCH_4 \geq 1$), but could be beneficial in terms of reducing temperature gradients, which can be pronounced in DIR. Although fuel recycling reduces the extent of the zone affected by carbon deposition, Figure 3 suggests that this problem may only be eliminated for fuel recycling ratios greater than approximately 50%.

As previously highlighted, methane fuels with low steam content would lower system requirements in terms of steam production, improve thermo-mechanical and materials reliability, as well as electrochemical performance (Figure 2). Figure 4 shows the predictions of coefficient γ at an inlet xH_2O/xCH_4 ratio of 0.5. This case highlights the potential value of anode gas recycling in terms of alleviating carbon deposition, although improvements are still required for low levels of recycling. In absence of recycling, almost two

thirds (18 mm) of the cell length analyzed would be susceptible to carbon deposits. For 20%, 40%, 60% and 80% fuel recirculation, the boundary of carbon deposition (defined as the location where γ becomes less than 1) is reduced to approximately 12 mm, 6 mm, 2 mm and 0.7 mm respectively. Although there is a clear improvement for 20% recirculation, the risk of carbon deposition is far from being eliminated. However at recycling ratios larger than on order 50%, only a minor portion of the cell is affected by coking, highlighting the potential benefit of this approach.

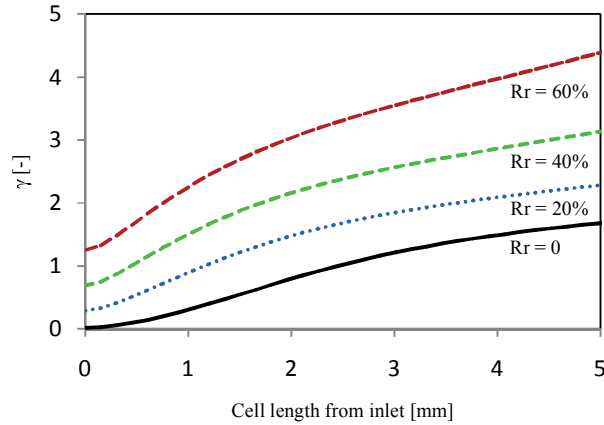


Figure 3. Numerically predicted profile of coefficient γ along the cell length direction, for an inlet fuel $x\text{H}_2\text{O}/x\text{CH}_4$ ratio of 1 and several fuel recycling ratios.

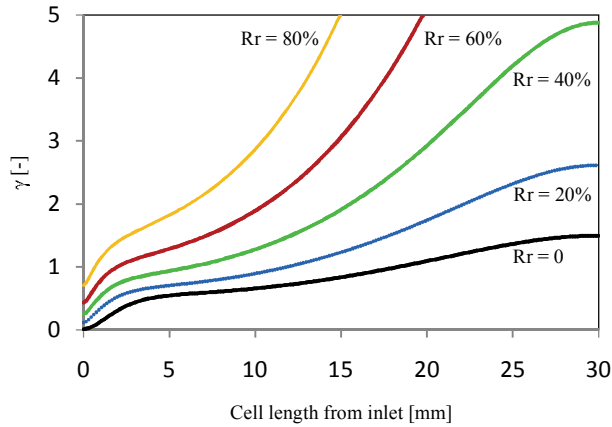


Figure 4. Numerically predicted profile of coefficient γ along the cell length direction, for an inlet fuel $x\text{H}_2\text{O}/x\text{CH}_4$ ratio of 0.5 and several fuel recycling ratios.

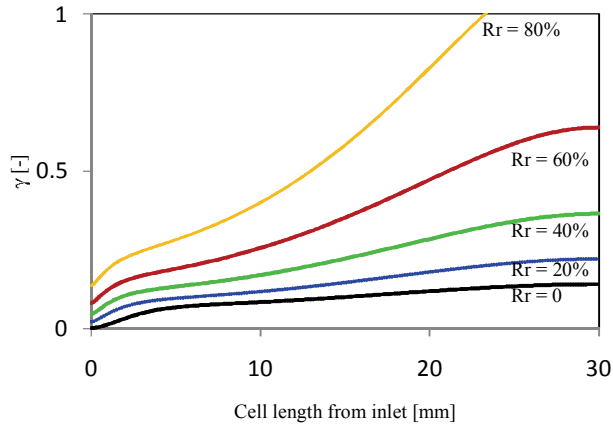


Figure 5. Numerically predicted profile of coefficient γ along the cell length direction, for an inlet fuel $x\text{H}_2\text{O}/x\text{CH}_4$ ratio of 0.1 and several fuel recycling ratios.

For a $x\text{H}_2\text{O}/x\text{CH}_4$ ratio of 0.1, the predictions of coefficient γ in Figure 5 indicate that even with high levels of anode gas recycling, most of, if not all of the cell length analyzed is affected by coking. It can therefore be concluded that partial fuel recycling alone would not be a viable strategy for dry or very weakly humidified hydrocarbon fuels. In such cases, fuel recirculation might help sustaining GIR operation and lower steam production requirements, but only when employed in tandem with other coking mitigation strategies. These may include an anode barrier layer or materials inhibitors to carbon deposition.

7. Conclusions

The challenges associated with carbon deposition in current Ni-YSZ based SOFCs operated on hydrocarbon fuels, and solutions previously explored in the literature were summarized. Using a detailed CFD model and thermodynamic analysis of the combined effects of the cracking and Boudouard reactions on the susceptibility to coking, the spatial extent of carbon deposits in a GIR-SOFC operated on humidified methane was quantified for several fuel humidification and recycling conditions.

At temperatures close to 1173 K and at inlet fuel $x\text{H}_2\text{O}/x\text{CH}_4$ ratios of 1, 0.5 and 0.1, the predictions indicate that in absence of fuel recycling, the anode region affected by carbon deposits represents approximately 8%, 60% and 100% of the length of the cell considered, respectively. This confirms that internal reforming is not sustainable for S:Cs less than unity in current Ni-YSZ anodes.

However, 50% (mass %) fuel recycling is found to be an effective mitigation strategy at inlet $x\text{H}_2\text{O}/x\text{CH}_4$ of 0.5 to 1, with only a minor portion of the cell inlet region affected by coking. For lower recycling ratios at the same fuel compositions, or lower $x\text{H}_2\text{O}/x\text{CH}_4$ ratios (regardless of the recycling ratio), fuel recycling reduces the risk of coking, but does not eliminate it. The results suggest that partial fuel recycling could contribute to extend the operational range of DIR-SOFCs to lower S:C ratios (0.5 to 1.0) than typically considered, with reduced risks of carbon deposition, while reducing system cost and complexity in terms of steam production. For dry or weakly humidified fuels, additional mitigation strategies would be required, such as an anode barrier layer or material inhibitor to carbon deposition, which alone may not suffice to systematically eliminate carbon deposits. Thus, a complete solution to carbon deposition in SOFCs fed on hydrocarbons may involve a combination of cell design and operating conditions.

Nomenclature

A/V	Specific catalyst surface per unit volume [m^{-1}]
a_c	Carbon activity [-]
d_{pore}	Pore diameter [m]
D_{ik}	Binary diffusion coefficient for species i and k [$\text{m}^2 \text{s}^{-1}$]
D_{ik}	ik component of the multi-component Fickian diffusivity matrix [$\text{m}^2 \text{s}^{-1}$]
$D_{ik,eff}$	Effective binary diffusivity for species i and k [$\text{m}^2 \text{s}^{-1}$]
E_0	Potential difference between the electrolyte and catalyst at equilibrium [V]
F	Faraday constant (96,500) [C mol^{-1}]
h_i	Enthalpy of the i th species [J kg^{-1}]
h_B	Solid phase enthalpy [J kg^{-1}]
$[i]$	Molar concentration of the i th species [kmol m^{-3}]
$[i]_0$	Reference concentration of the i th species [kmol m^{-3}]
I	Identity matrix [-]
j_{a0}	Anodic exchange current density [A m^{-2}]
j_{at}	Faradic current due to anodic reaction [A m^{-2}]
j_{c0}	Cathodic exchange current density [A m^{-2}]
j_{ct}	Faradic current due to cathodic reaction [A m^{-2}]
J_i	Diffusion flux of the i th species [$\text{kg m}^{-2} \text{s}^{-1}$]
K_B	Equilibrium constant of the Boudouard reaction [Pa^{-1}]
K_C	Equilibrium constant of the Cracking reaction [Pa]
M	Mean molar weight of the gas mixture [kg kmol^{-1}]
p	Total pressure [Pa]
P_i	Partial pressure of the i th species [Pa]

q	Heat flux [W m^{-2}]
r_k	Reaction rate of the k th reaction [$\text{kmol m}^{-3} \text{s}^{-1}$]
R	Universal gas constant (8.314) [$\text{J mol}^{-1} \text{K}^{-1}$]
R_i	Mass source term of species i through chemical/electrochemical reactions [$\text{kg m}^{-3} \text{s}^{-1}$]
R_r	Exhaust fuel mass recycling ratio [-]
$(S/V)_{eff}$	Effective TPB surface-to-volume ratio [$\text{m}^2 \text{m}^{-3}$]
T	Temperature [K]
\mathbf{v}	Fluid velocity vector [m s^{-1}]
ω_i	Mass fraction of the i th species [-]
ω_{i,in,R_r}	Mass fraction of the i th species at the fuel channel inlet for a fuel recycling ratio R_r [-]
ω_{i,out,R_r}	Mass fraction of the i th species at the fuel channel outlet for a fuel recycling ratio R_r [-]
x_i	Molar fraction of the i th species [-]

Greek letters

α	Boudouard coefficient [-]
α_a	Anodic Tafel constant [-]
α_c	Cathodic Tafel constant [-]
β	Cracking coefficient [-]
γ	Combined Boudouard and cracking coefficient [-]
ε	Porosity [-]
η_a	Anodic overpotential [V]
κ	Permeability of the porous medium [m^2]
λ	Effective thermal conductivity of the porous medium [$\text{W m}^{-1} \text{K}^{-1}$]
λ_B	Thermal conductivity of the solid phase [$\text{W m}^{-1} \text{K}^{-1}$]
λ_F	Thermal conductivity of the fluid [$\text{W m}^{-1} \text{K}^{-1}$]
μ	Dynamic viscosity of the gas mixture [Pa s]
μ_i	Dynamic viscosity of the i th species [Pa s]
ν_i	Reactional stoichiometric coefficient of the i th species [-]
ρ	Mass density of the gas mixture [kg m^{-3}]
ρ_B	Mass density of the solid phase [kg m^{-3}]
σ_{aS}	Ionic phase conductivity at anode [$\Omega^{-1} \text{m}^{-1}$]
σ_{aM}	Electronic phase conductivity at anode [$\Omega^{-1} \text{m}^{-1}$]
σ_{eS}	Ionic phase conductivity of the electrolyte [$\Omega^{-1} \text{m}^{-1}$]
τ	Pore tortuosity [-]
ϕ_{aS}	Ionic phase potential at anode [V]
ϕ_{aM}	Electronic phase potential at anode [V]
ϕ_{eS}	Ionic phase potential of the electrolyte [V]

Acknowledgements

The author wishes to thank Mr. Merwan Daoudi for his assistance in the model development, Dr. Yann Bultel and Mr. Jean-Marie Klein (Phelma-INPG, France) for clarifications on their previously published SOFC model, and COMSOL for their technical support.

References

- [1] Edwards, P.P. Kuznetsov, V. Johnson, S.R. Lodge, M.T.J. and Jones, M.O. 2006, "Sustainable Hydrogen Energy," in Future Electricity Technologies and Systems, Eds. Jamab, T. Nuttall, W.J. and Pollit, M.G., Cambridge University Press, Cambridge.
- [2] Song, C., 2002, "Fuel Processing for Low-Temperature and High-Temperature Fuel Cells Challenges, and Opportunities for Sustainable Development in the 21st Century", Catalysis Today, 77, pp. 17–49.

- [3] Krumpelt, M. Krause, T.R. Carter, J.D., Kopasz, J.P., and Ahmed, S., 2002, "Fuel Processing for Fuel Cell Systems in Transportation and Portable Power Applications", *Catalysis Today*, **77**, pp. 3–16.
- [4] Singhal, S.C. and Kendall, K., Eds., 2003, *High Temperature Solid Oxide Fuel Cells, Fundamentals, Design and Applications*, Elsevier, Oxford.
- [5] Peters, R., Dahl, R. Kluttgen, U., Palm, C., and Stolten, D., 2002, *Journal of Power Sources*, **106**, pp. 238–244.
- [6] Brandon, N.P., Skinner, S., and Steele, B.C.H., 2003, "Recent Advances in Materials for Fuel Cells", in *Annual Review of Materials Research*, Eds. Kreuer, K.D., Clarke, D.R., Ruhle, M., and Bravman, J.C., **33**, pp. 183-213.
- [7] Finnerty, C., Tompsett, G.A., Kendall, K., Ormerod, R.M., 2000, "SOFC system with integrated catalytic fuel processing", *Journal of Power Sources*, **86**, pp. 459-463.
- [8] Aguiar, P., Chadwick, D., Kershenbaum, L., 2002, "Modelling of an indirect internal reforming solid oxide fuel cell", *Chemical Engineering Science*, **57(10)**, pp. 1665–1677.
- [9] Laosiripojana, N. and Assabumrungrat, S., 2007, "Catalytic steam reforming of methane, methanol, and ethanol over Ni/YSZ: The Possible use of these Fuels in Internal Reforming SOFC", *Journal of Power Sources*, **163(2)**, Jan. 2007, pp. 943-951.
- [10] Clarke, S.H., Dicks, A.L., Pointon, K., Smith, T.A., and Swann, A., 1997, "Catalytic aspects of the steam reforming of hydrocarbons in internal reforming fuel cells", *Catalysis Today*, **38**, pp. 411–423.
- [11] Dicks, A.L., 1998, "Advances in catalysts for internal reforming in high temperature fuel cells", *Journal of Power Sources*, **71**, pp. 111-122.
- [12] Kim, T., Moon, S., Hong, S.I., 2002, "Internal carbon dioxide reforming by methane over Ni-YSZ-CeO₂ catalyst electrode in electrochemical cell", *Applied Catalysis A: General*, **224**, pp. 111-120.
- [13] Kawano, M., Matsui, T., Kikuchi, R., Yoshida, H., Inagaki, T., Eguchi, K., 2007, "Direct internal steam reforming at SOFC anodes composed of NiO-SDC composite particles", *Journal of the Electrochemical Society*, **154(5)**, pp. 460–465.
- [14] Irvine, J.T.S., and Sauvet, A., 2001, "Improved Oxidation of Hydrocarbons with New Electrodes in High Temperature Fuel Cells", *Fuel Cells*, **1(3-4)**, pp. 205-210.
- [15] Xu, J., Froment, G.F., 1989, "Methane steam reforming, methanation and water-gas-shift: I. Intrinsic kinetics", *American Institute of Chemical Engineers (A.I.Ch.E.) Journal*, **35**, pp. 88-96.
- [16] Amor, J.N., 1999, "The multiple roles for catalysis in the production of H₂", *Applied Catalysis, A*, **176**, pp. 159-176.
- [17] Klein, J.M., Bultel, Y., Pons, M., Ozil, P., "Modeling of a SOFC fuelled by methane: analysis of carbon deposition", *Transactions of the ASME, Journal of Fuel Cell Science and Technology*, **4(4)**, pp. 425-434.
- [18] Achenbach, E., 1994, "Three-dimensional and time-dependent simulation of a planar solid oxide fuel cell stack", *Journal of Power Sources*, **49(1-3)**, pp. 333–348.
- [19] Vernoux, P., Guindet, J., Kleitz, M., 1998, "Gradual internal methane reforming in intermediate-temperature solid-oxide fuel cells", *Journal of the Electrochemical Society*, **145(10)**, pp. 3487–3492.
- [20] Georges, S., Parrou, G., Henault, M., Fouletier, J., 2006, "Gradual internal reforming of methane: a demonstration", *Solid State Ionics*, **177(19-25)**, pp. 2109–2112.
- [21] Klein, J.M., Bultel, Y., Georges, S., Pons, M., 2007, "Modeling of a SOFC fuelled by methane: from direct internal reforming to gradual internal reforming", *Chemical Engineering Science*, **62(6)**, pp. 1636-1649.
- [22] Sun, C., Stimming, U., 2007, "Recent anode advances in solid oxide fuel cells", *Journal of Power Sources*, **171**, pp. 247-260.
- [23] Iida, T., Kawano, M., Matsui, T., Kikuchi, R., Eguchi, K., 2007, "Internal reforming of SOFCs, Carbon deposition on fuel electrode and subsequent deterioration of cell", *Journal of The Electrochemical Society*, **154(2)**, pp. B234-B241.
- [24] Wang, X., Gorte, R. J., 2002, "A study of steam reforming of hydrocarbon fuels on Pd/ceria", *Applied Catalysis A: General* **224(1-2)**, pp. 209-218.
- [25] Zhu, H., Colclasure, A., Kee, R., Lin, Y., Barnett, S., 2006, "Anode barrier layers for tubular solid-oxide fuel cells with methane fuel streams", *Journal of Power Sources*, **161(1)**, pp. 413–419.
- [26] Lin, Y., Zhan, Z., Liu, J., Barnett, S.A., 2005, "Direct operation of solid oxide fuel cells with methane fuel", *Solid State Ionics*, **176**, pp. 1827 – 1835.
- [27] Stiller, C., Thorud, B., Seljebo, S., Mathisen, O., Karoliussen, H., Bolland, O., 2005, "Finite-volume modeling and hybrid-cycle performance of planar and tubular solid oxide fuel cells", *Journal of Power Sources*, **141(2)**, pp. 227–240.

- [28] Colpan, C.O., Dincer, I., Hamdullahpur, F., 2007, “Thermodynamic modeling of direct internal reforming solid oxide fuel cells operating with syngas”, *International Journal of Hydrogen Energy*, **32(7)**, pp. 787-795.
- [29] Iwata, M., Hikosaka, T., Morita, M., Iwanari, T., Ito, K., Onda, K., Esaki, Y., Sakaki, Y., Nagata, S., 2000, “Performance analysis of planar-type unit SOFC considering current and temperature distributions”, *Solid State Ionics, Diffusion & Reactions*, **132(3-4)**, pp. 297-308.
- [30] Nikooyeh, K., Jeje, A.A., Hill, J.M., 2007, “3D modeling of anode-supported planar SOFC with internal reforming of methane”, *Journal of Power Sources*, **171(2)**, pp. 601–609.
- [31] Kee, R. J. Zhu, H. Sureshini, A. M., and Jackson, G. S., 2008, “Solid oxide fuel cells: operating principles, current challenges, and the role of syngas”, *Combustion Science and Technology*, **180(6)**, pp. 1207-1244.
- [32] Hou, K., Hughes, R., 2001, “The kinetics of methane steam reforming over a Ni/ α -Al₂O catalyst”. *Chemical Engineering Journal*, **82(1-3)**, pp. 311–328.
- [33] Pomfret, M.B., Owrutsky, J.C., Walker, R.A., 2007, “In situ studies of fuel oxidation in solid oxide fuel cells”, *Analytical Chemistry*, **79**, pp. 2367-2372.
- [34] COMSOL AB, 2007, *COMSOL Multiphysics Version 3.4 User’s Guide*.
- [35] Lehnert, W., Meusinger, J., Thom, F., 2000, “Modelling of gas transport phenomena in SOFC anodes”, *Journal of Power Sources*, **87**, pp. 57-63.
- [36] Young, J.B., 2007, “Thermofluid modeling of fuel cells”, *Annual Review of Fluid Mechanics*, **39**, pp. 193-215.
- [37] Shi, Y., Cai, N., Chen, L., Bao, C., Croiset, E., Qian, J., Hu, Q., Wang, S., 2007, “Modeling of an anode-supported Ni-YSZ|Ni-ScSZ|ScSZ|LSM-ScSZ multiple layers SOFC cell, Part I. Experiments, model development and validation”, *Journal of Power Sources*, **172**, pp. 235-245.
- [38] Bird, R.B., Byron, R., Stewart, W.E., Lightfoot, E.N., 2002, *Transport Phenomena*, 2nd. Ed., Wiley, New York.
- [39] Bosanquet, C.H., “British TA Report”, BR-507, 1944.
- [40] Bruggemann, D.A.G., 1935, “*Annalen der Physik*, **24**, pp. 636.
- [41] Westerterp, K.R., Van Swaaij, W.P.M., Beenackers, A.A.C.M., 1984, *Chemical reactor design and operation*.

Author Biography

Dr. Valérie Evely is an Assistant Professor in mechanical engineering specialized in thermofluids at The Petroleum Institute, United Arab Emirates. She holds a Ph.D. in mechanical engineering from Dublin City University, Ireland. Her present research interests are in renewable energies, with focus on solid oxide fuel cells for power generation in oil and gas industry applications, and engineering education. Prior to joining the Petroleum Institute, she was with several divisions of Nokia, including Nokia Research Center, Finland, Electronics Thermal Management, Ireland, and the CALCE EPSC at the University of Maryland, USA. She has over fourteen years experience in the packaging, thermal management and reliability of electronic equipment, computational fluid dynamics and biomedical human health monitoring. She has authored or co-authored over 50 refereed journal and conference publications and two book chapters, and is a co-editor of the First Energy 2030 conference proceedings. Dr. Evely is a member of several international conference program committees focused on energy technologies, electronics reliability and thermal phenomena in electronic systems.